Advanced Deep Learning for Multi-View Structural Reasoning in Mammographic Analysis

Internship Overview

Student : Imade Bouftini
Supervision : Youssef ALJ

October 20, 2025

Overview

1. Clinical Context & Problem Statement
2. Single-view detection
3. Multi-view detection
4. Results & comparison
5. Conclusion & Perspectives

Section I

Introduction

- Breast cancer affects millions worldwide (2.3M new cases annually)
- Early detection can reduce mortality by 20-40%
- Mammography is the primary screening tool

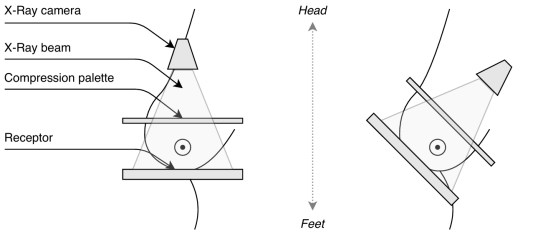

Imaging protocol [Source]

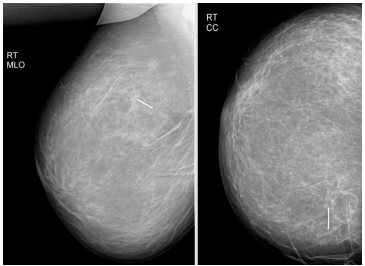

Mammogram Views (MLO/CC)

Clinical Context: Detection Challenges
Balancing Sensitivity and Specificity in Screening

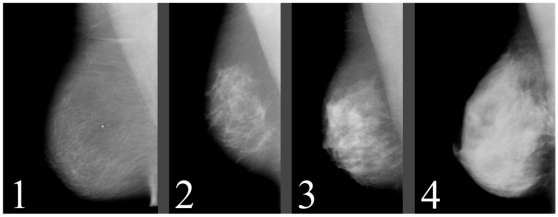

Figure: Mammograms with various density levels [Source]

Clinical Challenges:

- Diverse tissue density and appearance variation between patients
- Extremely low prevalence ($\sim 0.5\%$ in screening populations)
- Subtle presentation of early-stage cancers

False negatives cause:

- Delayed diagnosis
- Poorer prognosis
- Increased treatment costs

False positives cause:

- Unnecessary biopsies
- Patient anxiety and stress
- Healthcare resource burden

Core Challenge

How can we leverage ipsilateral and bilateral views to replicate the natural reasoning ability of radiologists in breast cancer detection?

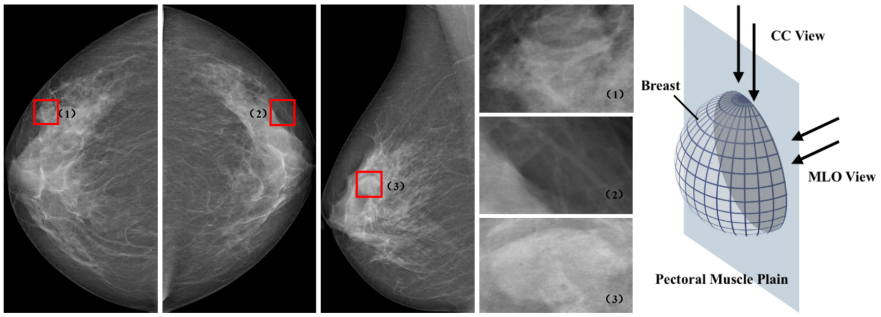

(a) Examined view (b) Contralateral view (c) Auxiliary view (d) Zoom-in patches (e) Ideal projection model

Figure: Illustration of the relation among mammography views [Source]

Section II

Single-view detection

SOTA Single-View Detection Models

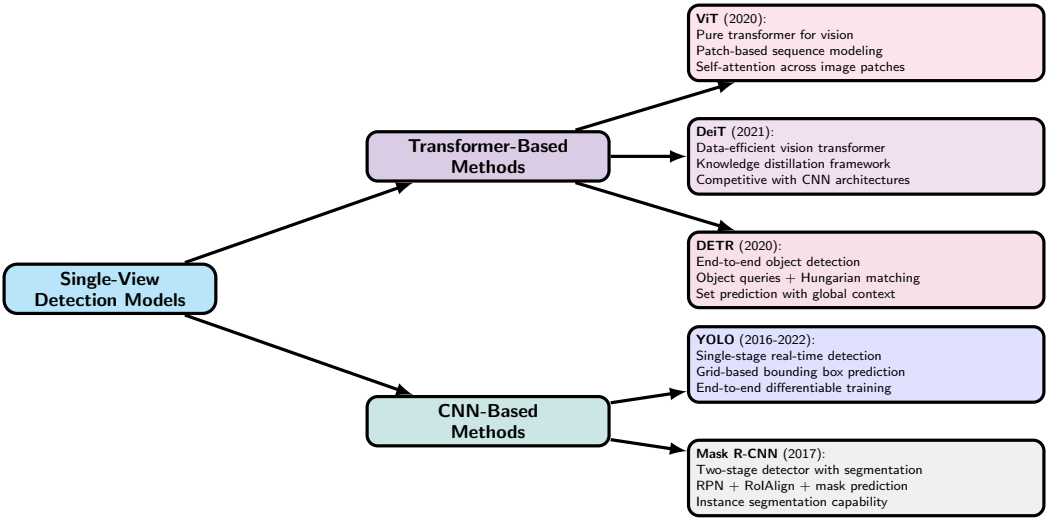

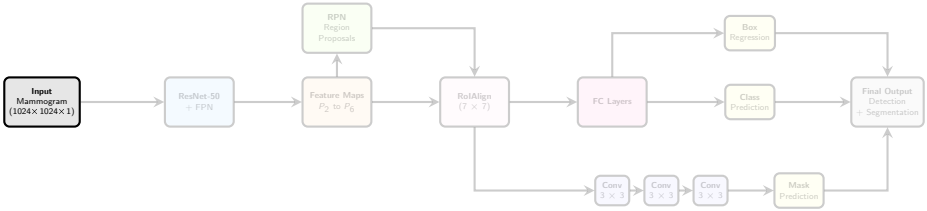

Step 1: Data Preparation

Data Loading

Mammogram Standardization:

- Let $I_{\text{raw}} \in \mathbb{N}^{H \times W}$ coded in `uint16`
- Normalized image: $I_{\text{norm}} = \frac{I_{\text{raw}}}{65535}$ then $I_{\text{norm2}} = \frac{I_{\text{norm}} - m_{imagenet}}{\sigma_{imagenet}}$
- Resized to 1024×1024

Medical Augmentation Pipeline

- **Elastic Distortion**: tissue deformation and compression variations
- **RandomGamma**: exposure variations between mammographs
- **GaussianBlur**: focus variations
- **GaussNoise**: sensor noise
- **RandomBrightnessContrast**: illumination differences
- **Geometric transformations**: handle different orientations

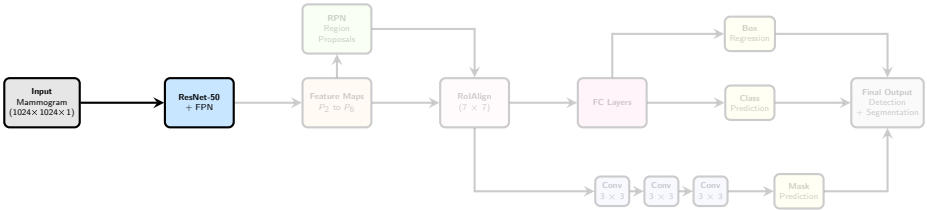

Step 2: Backbone Feature Extraction (ResNet-50)

ResNet-50

Backbone: Extracts high-level semantic features using a ResNet-50 pretrained on ImageNet.

Residual Blocks: Solve the vanishing gradient problem by adding skip connections.

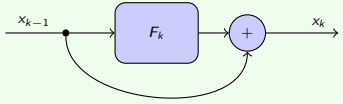

$$x_k = F_k(x_{k-1}) + x_{k-1}$$

Transform Parameters

Input Adaptation for Grayscale:

- ImageNet weights assume RGB input.
- Grayscale adaptation via channel-wise averaging:

$$W_{\text{gray}} = 0.299.W_R + 0.587.W_G + 0.114.W_B$$

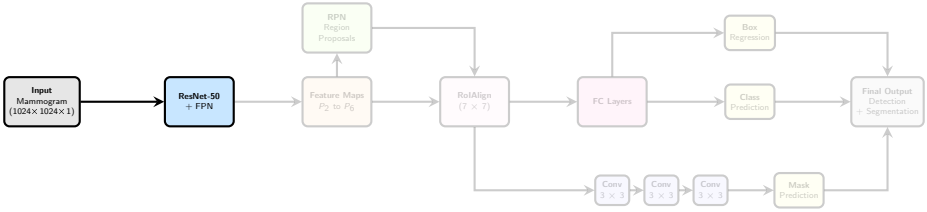

Step 3: Feature Pyramid Network (FPN)

Feature Pyramid Network

Bottom-up: C_2 to C_5 with strides $\{4, 8, 16, 32\}$
Top-Down Path: $P_i = C_i + \text{Upsample}(P_{i+1})$
Multi-Scale Features:

- P_2: Microcalcifications (5-15px)
- P_3: Small masses (15-40px)
- P_4: Medium masses (40-100px)
- P_5: Large masses (100-250px)

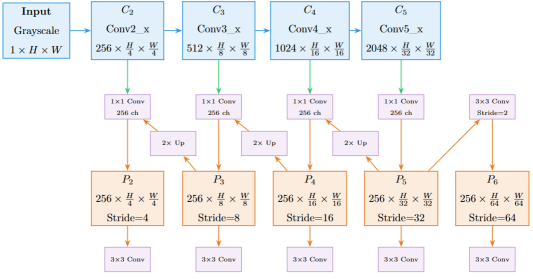

Figure: FPN architecture overview

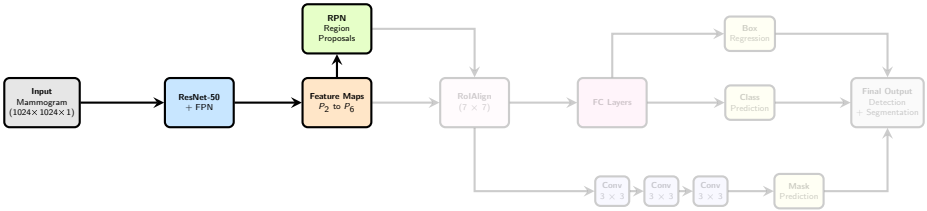

Step 4: Region Proposal Network (RPN)

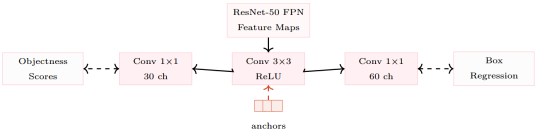

Figure: RPN architecture overview

RPN Loss Function

$$L_{rpn} = \frac{1}{N_{cls}} \sum_i L_{cls}(p_i, p_i^*) + \frac{\lambda}{N_{reg}} \sum_i p_i^* L_{reg}(t_i, t_i^*)$$

- $L_{reg}(t, t^*) = \text{smooth}_{\ell_1}(t - t^*)$
- $L_{cls}(p_i, p_i^*) = -p_i * log(p_i) - (1 - p_i^*) log(1 - p_i)$

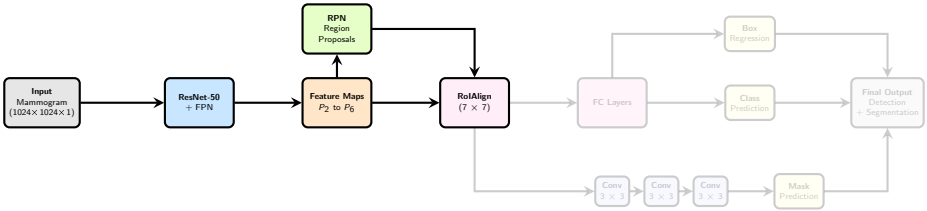

Step 5: RoIAlign

RoIAlign Implementation

Bilinear Interpolation:

$$f(x, y) = \sum_{i,j} f(i, j) \max(0, 1 - |x - i|) \max(0, 1 - |y - j|)$$

Quantization-Free Alignment:

- No coordinate snapping
- Sub-pixel accuracy maintained
- 7×7 output resolution
- Critical for mask precision

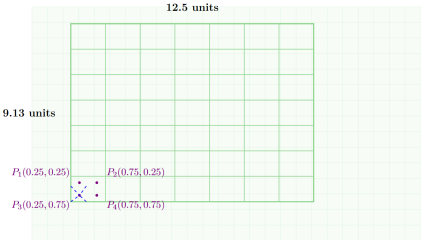

Figure: RoIAlign illustration example

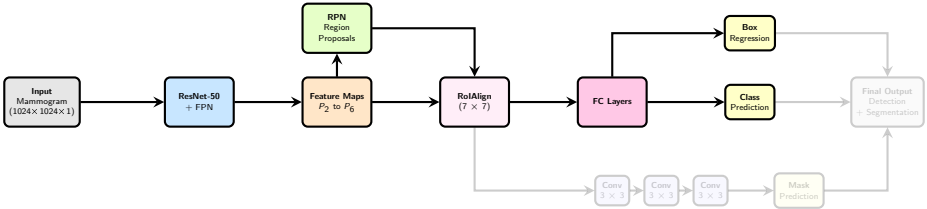

Step 6: Classification and Box Regression

Classification + Box Regression

FC Architecture:

$$p = \text{softmax}(W_{cls} \cdot f + b_{cls})$$

$$\Delta = W_{box} \cdot f + b_{box}$$

Network Structure:

- FC1: $7 \times 7 \times 256 \rightarrow 1024$
- FC2: $1024 \rightarrow 1024$
- Class output: $1024 \rightarrow 2$ (background + mass)
- Box output: $1024 \rightarrow 4$ coordinates

Box Parameterization

Regression Targets:

- $t_x = (x - x_a)/w_a$
- $t_y = (y - y_a)/h_a$
- $t_w = \log(w/w_a)$
- $t_h = \log(h/h_a)$

Smooth ℓ_1 and CE as losses

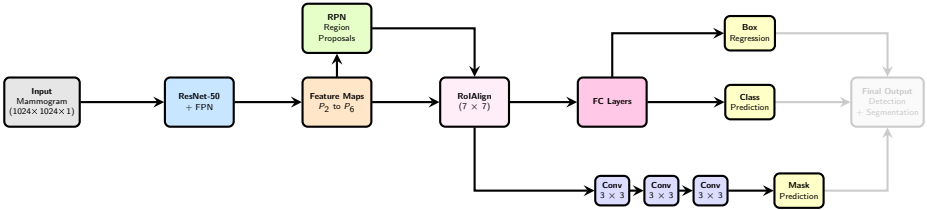

Step 7: Segmentation

Mask Head Architecture

Convolutional Stack:

- 4x Conv3x3-256-ReLU layers
- Deconv2x2: 256 $\rightarrow$ 2 classes
- Output: $14 \times 14 \times 2$ binary masks
- Per-class mask prediction
- Sigmoid activation for binary output

Mask Loss

$$L_{mask} = -\frac{1}{m^2} \sum_{i,j} [y_{ij} \log(\hat{y}_{ij}) + (1 - y_{ij}) \log(1 - \hat{y}_{ij})]$$

- Computed only for positive ROIs
- Binary cross-entropy per pixel

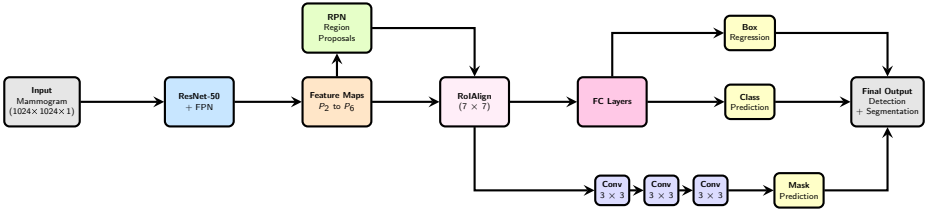

Step 8: Training on Multi-Task Loss

Multi-Task Loss

$$L_{total} = L_{rpn} + L_{det} + L_{mask}$$

Training Configuration:

- Weight decay: 10^{-4}
- Momentum: 0.9
- Gradient clipping: $\|\nabla\| \leq 1.0$
- Batch size: 2 images

3-stage training

1. heads for 10 epochs (LR=0.002)
2. Initial backbone layers (LR=0.0005)
3. Full network for 5 epochs (LR=0.0001)

Section III

Multi-view detection

SOTA Multi-View Detection Models

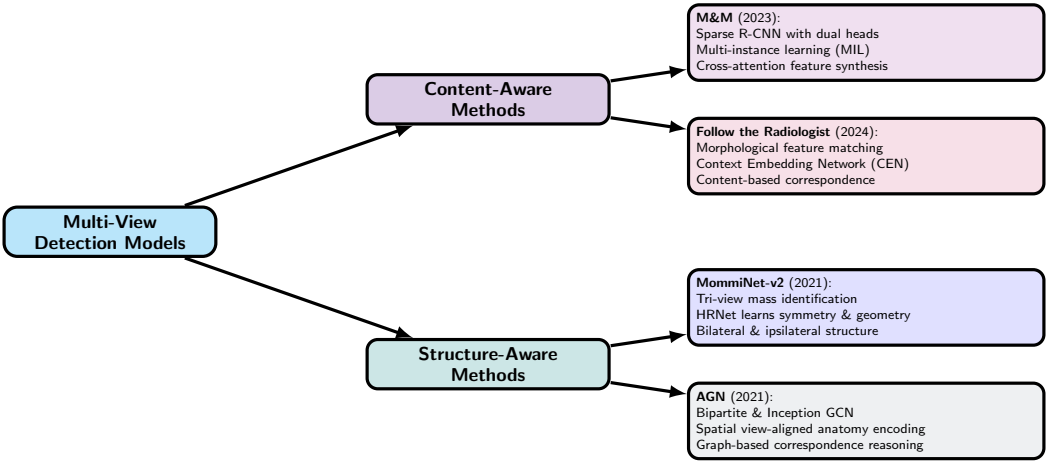

MaskRCNN adaptation for multi-view detection

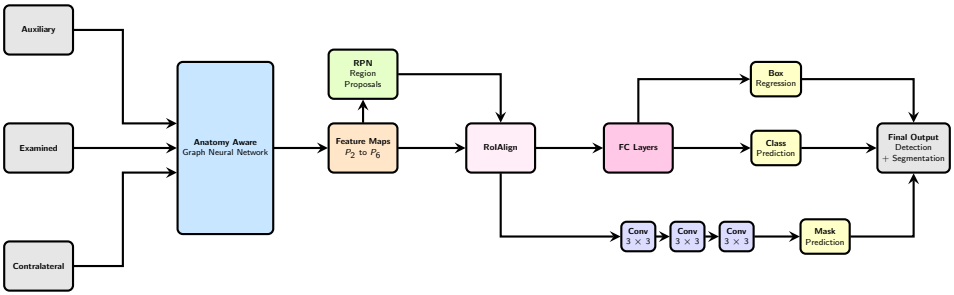

To enable multi-view reasoning, **we replace the standard backbone with an Anatomy-Aware GCN** that fuses auxiliary/contralateral features into the examined view

Anatomy-aware Graph Network: Core Idea

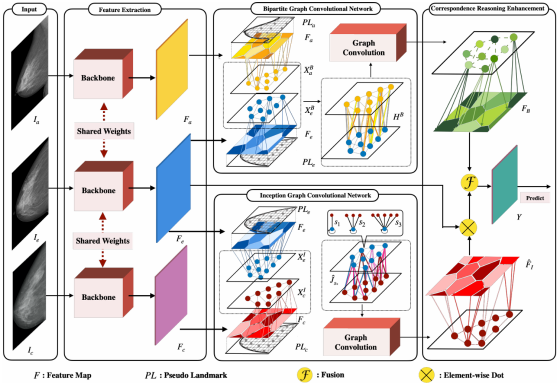

Figure: AGN architecture [Source]

Key Idea

AGN models **multi-view anatomical reasoning** by explicitly encoding correspondences across:

- **Ipsilateral views** (CC & MLO of the same breast)
- **Bilateral views** (CC-left vs. CC-right or MLO-left vs. MLO-right)

Key structure

The network uses two Graph Convolutional Networks (GCNs):

- **BGN**: Bipartite Graph for ipsilateral reasoning
- **IGN**: Inception Graph for bilateral symmetry analysis

Graph construction : Pseudo landmarks

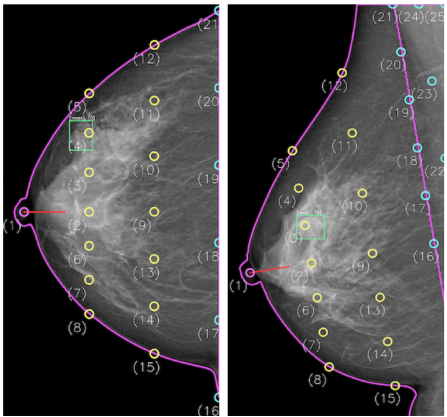

(a) CC View (b) MLO View

Figure: Pseudo landmarks in MLO/CC views [Source]

Definition

Pseudo landmarks $\mathcal{V} = \{v_i\}_{i=1}^{N}$ are consistent reference points on mammograms.

- Placed using anatomical priors: nipple, pectoral line and breast contour
- Ensure consistent correspondence across patients
- Used to define nodes in both GCNs

Why Not Grids?

Uniform grids are sensitive to scale, shape, and orientation. Pseudo landmarks preserve anatomical semantics.

1. Breast Region Segmentation (Otsu's Method):

$$t^* = \arg\max_t \{\omega_0(t)\omega_1(t)[\mu_0(t) - \mu_1(t)]^2\} \tag{1}$$

2. Contour Smoothing (B-spline):

$$S(u) = \sum_{i=0}^{n-1} P_i B_i(u) \tag{2}$$

Optimization objective:

$$\min_S \left\{ \sum_{i=1}^{n} |C_i - S(u_i)|^2 + s \int_0^1 |S''(u)|^2 du \right\} \tag{3}$$

Adaptive smoothing parameter:

$$s = \begin{cases} 10^7 & \text{if view = MLO} \\ 100 & \text{if view = CC} \end{cases} \tag{4}$$

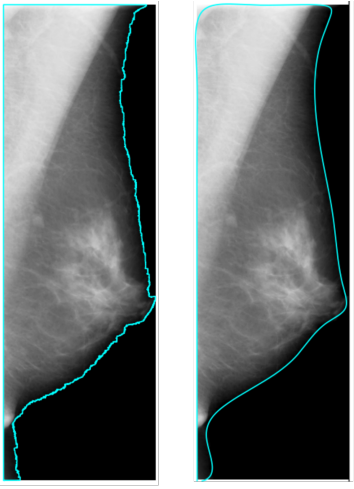

Contour extraction and smoothing: Raw extracted contour vs. smoothed contour with B-spline interpolation

1. CC View Detection (Lateralmost Point):

$$p_{nipple} = \begin{cases} \arg\min_i x_i & \text{if side} = \text{Right} \\ \arg\max_i x_i & \text{if side} = \text{Left} \end{cases} \tag{5}$$

2. MLO View Detection:
Candidate Selection (Lower Lateral Quadrant):

$$\begin{cases} x \geq 0.75w \text{ and } y \geq 0.5h & \text{if Left} \\ x \leq 0.25w \text{ and } y \geq 0.5h & \text{if Right} \end{cases} \tag{6}$$

Curvature Analysis:

$$\kappa(u) = \frac{x'(u)y''(u) - y'(u)x''(u)}{(x'(u)^2 + y'(u)^2)^{3/2}} \tag{7}$$

Optimal Selection:

$$\text{score}(i) = |\kappa(u_i)| \tag{8}$$

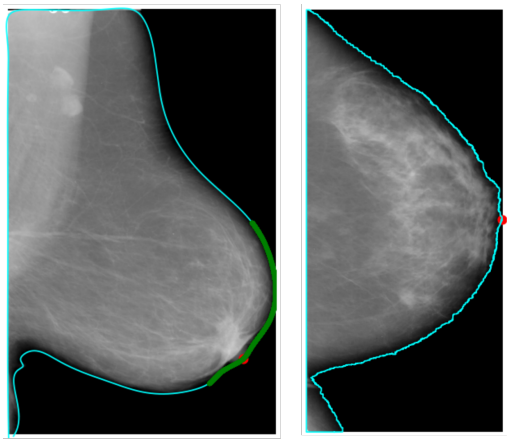

Nipple detection: (a) MLO curvature analysis with candidates (green) and final nipple (red) (b) CC lateralmost point detection

1. CC View (Vertical Line Approximation):

$$x_{pectoral} = \begin{cases} \min_i x_i & \text{if side = Left} \\ \max_i x_i & \text{if side = Right} \end{cases} \tag{9}$$

2. MLO View (8-Stage Pipeline):
ROI Definition:

$$\text{ROI} = \begin{cases} [0,\, 0.4w] \times [0,\, 0.6h] & \text{if Left} \\ [0.6w,\, w] \times [0,\, 0.6h] & \text{if Right} \end{cases} \tag{10}$$

CLAHE Enhancement:

$$I_{CLAHE} = \text{CLAHE}(I_{ROI},\, \text{clipLimit} = 3.0,\, \text{tileGridSize} = (8, 8)) \tag{11}$$

Combined Thresholding:

$$T_{Combined} = \text{Otsu}(I_{CLAHE}) \wedge \text{AdaptiveThreshold}(I_{CLAHE}) \tag{12}$$

Hough Line Detection:

$$L = \text{HoughLinesP}(E,\, \rho = 1,\, \theta = \pi/180,\, \text{threshold} = 20) \tag{13}$$

Slope Filtering:

$$\text{valid}(L_i) = \begin{cases} \text{slope}(L_i) < 0 & \text{if Left} \\ \text{slope}(L_i) > 0 & \text{if Right} \end{cases} \tag{14}$$

Line Scoring:

$$\text{score}(L_i) = \text{length}(L_i) \cdot (w_{pos} \cdot \text{pos\_score} + w_{angle} \cdot \text{angle\_score}) \tag{15}$$

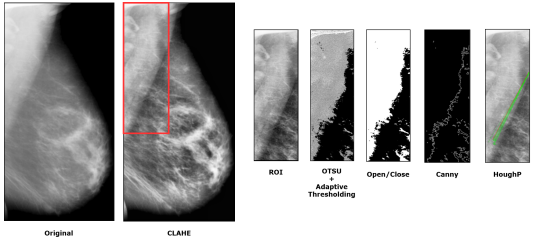

Pectoral muscle detection pipeline: (a) Original MLO (b) ROI+CLAHE (c) Thresholding (d) Morphological ops (e) Edge detection (f) Line candidates (green) and final line (red)

Landmark Detection: Graph Construction
Parallel Lines and k-NN Node Mapping

1. Parallel Line Generation:

$$\vec{v}_{pect} = \frac{\vec{p}_{pect2} - \vec{p}_{pect1}}{|\vec{p}_{pect2} - \vec{p}_{pect1}|}$$

$$\vec{p}_{line1} = \vec{p}_{nipple} + \frac{1}{3}|\vec{p}_{intersect} - \vec{p}_{nipple}| \cdot \vec{v}_{nipple-pect} \tag{16}$$

$$\vec{p}_{line2} = \vec{p}_{nipple} + \frac{2}{3}|\vec{p}_{intersect} - \vec{p}_{nipple}| \cdot \vec{v}_{nipple-pect}$$

2. Corner Line (MLO Views):

$$\vec{p}_{corner} = \begin{cases} (0,0) & \text{if side = Left} \\ (w-1,0) & \text{if side = Right} \end{cases} \tag{17}$$

$$\vec{p}_{corner\_line} = \vec{p}_{pect\_top} + \frac{1}{2}|\vec{p}_{corner} - \vec{p}_{pect\_top}| \cdot \vec{v}_{perpendicular} \tag{18}$$

3. Node Distribution:

$$\vec{p}_{node\_i} = \vec{p}_{start} + \frac{i}{k-1}(\vec{p}_{end} - \vec{p}_{start}), \quad i \in \{0, 1, \ldots, k-1\} \tag{19}$$

4. k-NN Node Mapping:

$$\phi_k(F, V) = (Q_f)^T F \quad Q_f = A(\Lambda_f)^{-1} \tag{20}$$

$$A_{ij} = \begin{cases} 1 & \text{if } j\text{th node is among } k \text{ nearest of } i\text{th pixel} \\ 0 & \text{otherwise} \end{cases} \tag{21}$$

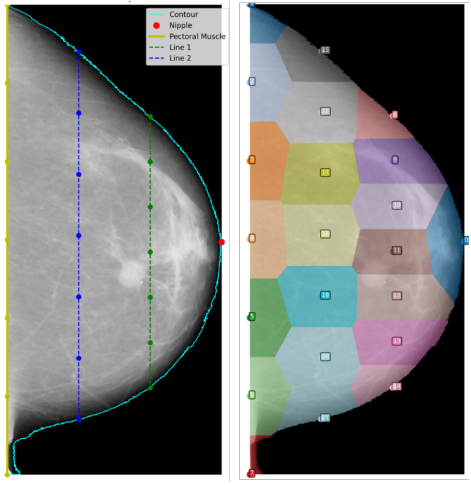

Graph construction: (a) CC view with landmarks and parallel lines (b) k-NN segmented regions mapping spatial features to graph nodes

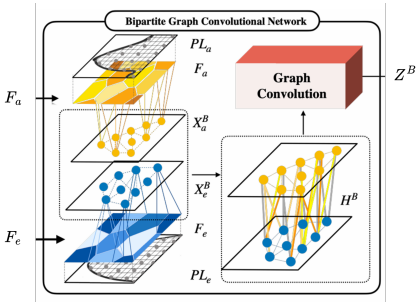

BGN Structure

Bipartite Graph Network models relationships between corresponding regions in CC and MLO views:

- **Nodes:** Pseudo landmarks in each view
- **Edges:** Connect nodes across views (CC to MLO)

Feature Extraction

Node features from backbone:

$$X_e^B = \phi_k(F_e, \mathcal{V}_{l_e}), \quad X_a^B = \phi_k(F_a, \mathcal{V}_{l_a})$$

Edge Weighting

Combines geometric and semantic information:

$$H = H_g \circ H_s$$

Geometric Relations (H_g)

Statistical co-occurrence from training data:

- Mass instances guide correspondence
- Normalized to prevent skew:

$$H_{ij}^{g} = \frac{\epsilon_{ij}}{\sqrt{D_{i\cdot} D_{\cdot j}}}$$

Semantic Relations (H_s)

Learnable appearance similarities:

- Feature fusion to model similarity:

$$H_{ij}^{s} = \sigma\left(\left[\left(X_i^{CC}\right)^T, \left(X_j^{MLO}\right)^T\right] w_s\right)$$

- Adapts to individual patient characteristics

Graph Message Passing

Information propagation across views via adjacency matrix:

$$Z^B = \sigma(H^B X^B W^B)$$

BGN Compoenents

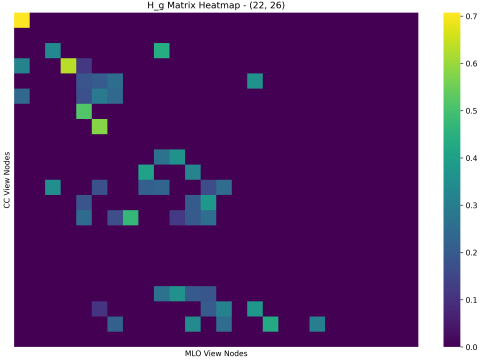

Figure: Geometric similarity matrix heatmap resulting from frequency calculation over the CBIS-DDSM training split

- We find that the nipple area H_{11}^{g} has the strongest correlation.
- We also find that there is no association in the pectoral muscle nodes, indicating that the presence of a mass in this location is unlikely.
- This matrix is calculated in advance which is time and memory efficient.

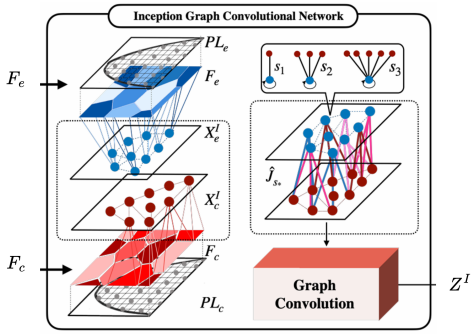

Key Insight

Asymmetry between left and right breasts is a key radiological clue:

- Healthy breasts show structural symmetry
- Suspicious masses create asymmetry

Inception Architecture

Multi-branch connections handle geometric distortions:

- s_1, s_2, s_3 nearest neighbor branches
- Each connects different neighbor counts
- Tolerates normal anatomical variation

Multi-branch Adjacency (J_s)

Inception architecture with multiple neighborhood sizes:

- Each branch s_i connects to top-s_i nearest neighbors
- Tolerance for geometric distortions:

$$J_{s_i}(m,n) = \begin{cases} 1 & \text{if } n \in \text{top-}s_i\text{NN}(m) \\ 0 & \text{otherwise} \end{cases}$$

Asymmetry Detection

Output highlights regions showing bilateral asymmetry:

- Attention maps guide detection
- Robust across breast densities
- Tolerates anatomical variations

Graph Message Passing

Multi-branch information propagation:

$$Z^l = \sigma\left(\begin{pmatrix} \hat{J}_{s_1} & \hat{J}_{s_2} & \hat{J}_{s_3} \end{pmatrix} \begin{pmatrix} X^l & \mathbf{0} & \mathbf{0} \\ \mathbf{0} & X^l & \mathbf{0} \\ \mathbf{0} & \mathbf{0} & X^l \end{pmatrix} \begin{pmatrix} W_1^l \\ W_2^l \\ W_3^l \end{pmatrix} \right)$$

Where $X^l = [(X_e^l)^T, (X_c^l)^T]^T$ combines examined and contralateral node features.

Graph to Spatial Projection

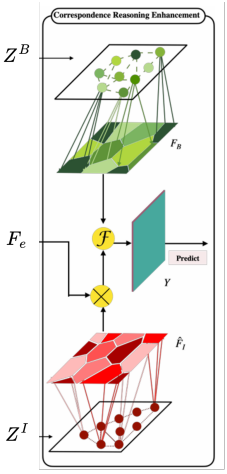

kNN Reverse Mapping ψ_k

Projects node features back to image space:

$$F^B = \psi_k(Z^B, \mathcal{V}_e), \quad F^I = \psi_k(Z^I, \mathcal{V}_e)$$

For each pixel, weighted average of k-nearest nodes.

Attention Application

IGN produces spatial attention map for examined view:

$$\hat{F}^I = \sigma(F^I w_I)$$

Highlights regions showing asymmetry with contralateral breast.

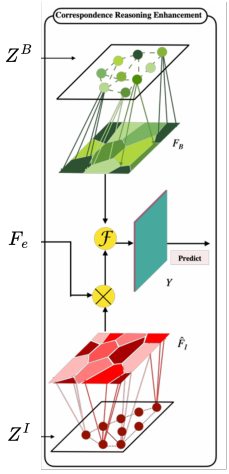

Final Feature Enhancement

Combined multi-view reasoning:

$$Y = [\hat{F}_I \circ F_e, F_B] W_f^\top$$

Where:

- $\hat{F}_I \circ F_e$: Attention-weighted examined features
- F_B: Ipsilateral correspondences
- W_f: Fusion layer parameters

Section IV

Results & Comparison

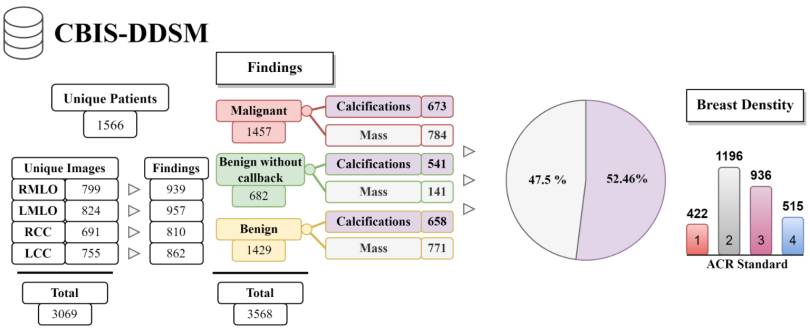

Figure: The CBIS-DDSM database statistics [Source]

Key Statistics: 1,566 unique patients • 3,069 mammographic images • 3,568 annotated findings

Finding Distribution: 1,457 malignant cases, 2,111 benign cases across four mammographic views (RMLO, LMLO, RCC, LCC) with varying breast density classifications (ACR 1-4).

Mammogram

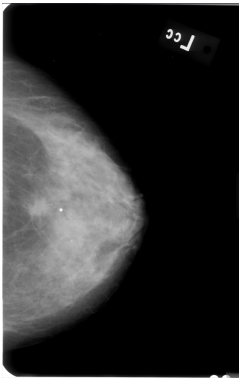

Original breast X-ray image

ROI

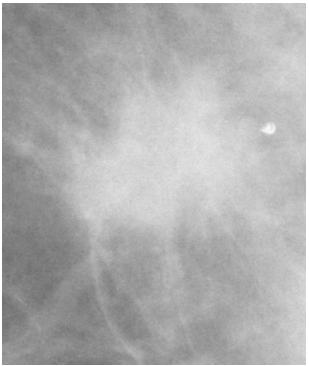

Cropped area

Mask

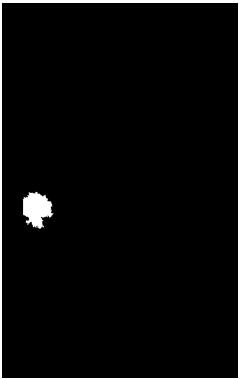

Binary segmentation mask

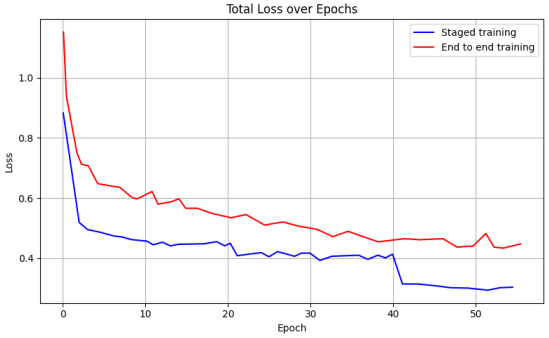

Figure: Total loss comparison between 3-stage training and end-to-end training

- **Staged Training Advantage:** Drops at each transition from one stage to another, rather than early plateau
- **Better Convergence:** Staged training achieves lower final loss compared to end-to-end approach
- **Training Stability:** Noise due to small batch size (2) for memory constraints accommodation
- **Progressive Learning:** Each stage builds upon previous knowledge systematically

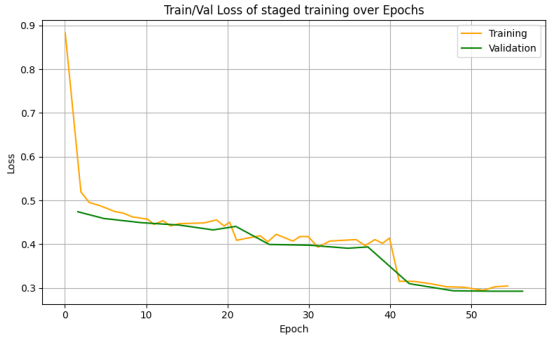

Figure: Comparison between training and validation losses in 3-stage training

- **Proper Fitting:** Validation loss follows training loss pattern
- **Smoother Validation:** Computed every two epochs to optimize computational resources
- **Convergence Success:** Both losses stabilize at acceptable levels

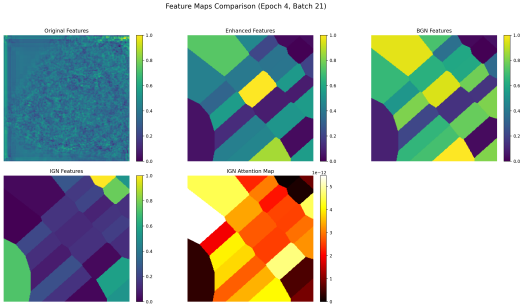

Figure: AGN Features with staged training before model adjustments

- **Destructive Attention:** IGN attention values approaching zero (scale: 10^{-12})
- **Feature Elimination:** Original multiplicative approach: $F_{enhanced} = \sigma(F_I \mathbf{w}_I) \odot F_e$
- **Training Instability:** Randomly initialized weights disrupted pre-trained MaskRCNN features
- **Performance Degradation:** Unable to recover initial MaskRCNN performance levels

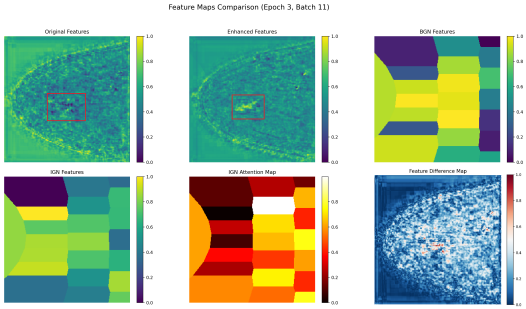

Figure: AGN Features with staged training after model adjustments

- **Background Suppression:** Enhanced features show reduced activation in irrelevant regions (breast contour, background)
- **Mass Enhancement:** Target lesion regions exhibit stronger, more focused activation
- **Residual Attention:** $F_{enhanced} = F_e \odot (2\hat{F}_I + 0.2)$ enables both suppression and enhancement
- **Feature Preservation:** 20% residual connection maintains base features even with minimal attention

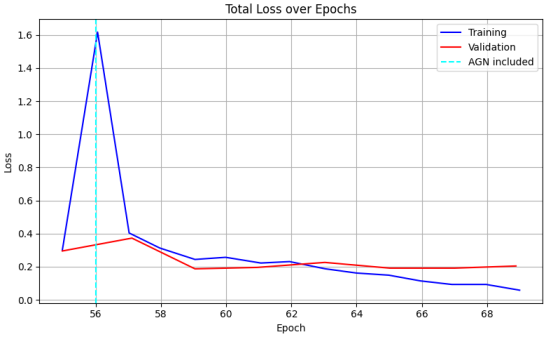

Figure: Training and Validation losses after AGN integration

- **Integration Point:** Training begins at epoch 56 (post-MaskRCNN training)
- **Initial Spike:** Loss peak due to arbitrary feature representation impact at start
- **Rapid Improvement:** Significant loss decrease achieving better results than MaskRCNN alone
- **Early Stopping:** Implemented at epoch 62 due to overfitting (87 training, 24 validation samples)

Table: Component-wise Performance Analysis on CBIS-DDSM (%).

Method	R@0.5	R@1.0	R@2.0	R@3.0	R@4.0
MaskRCNN (Baseline)	68.9	79.8	86.3	90.2	91.3
+ BGN only	72.1	81.5	87.8	90.8	91.7
+ IGN only	71.3	82.2	88.1	90.5	91.9
+ AGN (Original fusion)	54.2	63.1	68.9	71.1	72.0
+ AGN (Our modifications)	**78.4**	**85.5**	**90.1**	**91.6**	**92.5**

Table: Pseudo-Landmark Density Analysis on CBIS-DDSM (%).

Configuration	R@0.5	R@1.0	R@2.0	Notes
PL(13, 17)	76.8	84.1	89.3	Sparse configuration
PL(22, 26)	**78.4**	**85.5**	**90.1**	**Optimal density**
PL(100, 105)	77.2	84.8	89.7	Over-parameterized

Table: Graph Node Mapping Parameter Analysis on CBIS-DDSM (%).

Mapping Strategy	R@0.5	R@1.0	R@2.0	Notes
kNN, k=1 (Voronoi)	75.2	83.8	88.9	Nearest neighbor only
kNN, k=3	**78.4**	**85.5**	**90.1**	**Optimal context**
kNN, k=5	77.8	84.9	89.7	Over-smoothed features

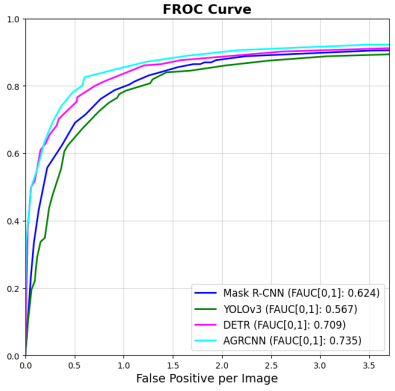

Figure: Comparative FROC analysis between MaskRCNN, YOLO, DETR and AGRCNN

- **Superior Performance:** AGRCNN clearly outperforms all single-view models
- **High Sensitivity:** Achieves high recall without generating additional false positives
- **Model Convergence:** All models converge at high FPI due to increased detection boxes

Model	0.5 FPI	1.0 FPI	2.0 FPI	3.0 FPI	4.0 FPI	Dataset	Images
Reference Paper (ALR) Results							
ALR MaskRCNN+FPN	83.1%	88.0%	91.4%	93.4%	94.2%	DDSM	2,620
ALR AG-RCNN	87.6%	90.6%	93.4%	94.7%	95.2%	DDSM	2,620
ALR Improvement	*+4.5%*	*+2.6%*	*+2.0%*	*+1.3%*	*+1.0%*		
Our Implementation Results							
Our MaskRCNN+FPN	68.9%	79.8%	86.3%	90.2%	91.3%	CBIS-DDSM	1,560
Our AGRCNN	78.4%	85.5%	90.1%	91.6%	92.5%	CBIS-DDSM	1,560
Our Improvement	*+9.5%*	*+5.7%*	*+3.8%*	*+1.4%*	*+1.2%*		
Difference	**+5.0%**	**+3.1%**	**+1.8%**	**+0.1%**	**+0.2%**		**(-40%)**

Table: AGRCNN Performance Enhancement Comparison with Dataset Information

- **Consistent Enhancement:** AGN provides substantial recall improvements across all FPI levels
- **Existing bias:** MaskRCNN of ALR had less room for improvement because it has already been trained on a large dataset

Section V

Conclusion & Perspectives

Conclusion & Perspectives

Key Takeaways

- **Clinically Meaningful Improvements**: Multi-view detection models outperform drastically the single-view models at performance. 9.5% recall gain $\implies \sim 47$ fewer missed cancers per 1000 screens
- **Data Challenge**: they are constrained by the requirement of big datasets with multiple mammograms per patient

Future Directions

- Training AGRCNN on larger datasets and compare it with other SOTA multi-view methods
- Develop a malignancy classification model (ResNet+CBAM, InceptionV3, etc.)

Opening

- Multi-view models are inherently limited as they try to predict a 3D mass from 2D projections
- This motivates the reconstruction of dense representations like DBT or MRI using neural representations and perform detection in 3D

Thank you for your attention

Questions?

Student: Imade Bouftini
Supervision: Youssef ALJ

AI Movement
Mohammed VI Polytechnic University
October 20, 2025

Appendix

- DETR architecture overview
- DDSM cleaning
- Anchors optimization in MaskRCNN
- GPU training details

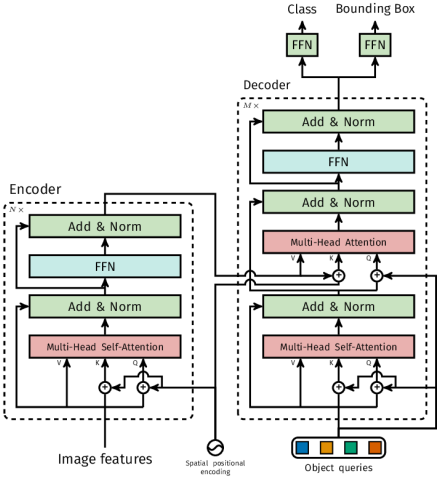

Figure: DETR architecture overview

Step 1: Feature Extraction & Positional Encoding

CNN Backbone

ResNet-50 Feature Extraction:

- Input: $\mathbf{x}_{img} \in \mathbb{R}^{H \times W \times 1}$
- CNN features: $\mathbf{f} \in \mathbb{R}^{H/32 \times W/32 \times C}$
- Lower resolution but rich semantics
- $C = 2048$ for ResNet-50

Positional Encoding

Spatial Position Information:

$$\mathbf{f}_{final} = \mathbf{f} + \mathbf{pos}$$

- Sine/cosine positional encoding
- Essential for spatial reasoning
- $\mathbf{pos} \in \mathbb{R}^{H/32 \times W/32 \times C}$
- Enables transformer to understand spatial layout

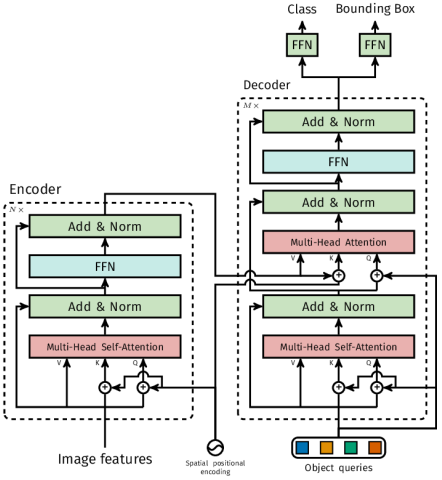

Figure: DETR architecture overview

Step 2: Transformer Encoder

Self-Attention Mechanism

Multi-Head Self-Attention:

$$\text{MSA}(\mathbf{X}) = \text{Concat}(\text{head}_1, \ldots, \text{head}_h)\mathbf{W}^O$$

$$\text{head}_i = \text{Attention}(\mathbf{X}\mathbf{W}_i^Q, \mathbf{X}\mathbf{W}_i^K, \mathbf{X}\mathbf{W}_i^V)$$

Where:

$$\text{Attention}(\mathbf{Q}, \mathbf{K}, \mathbf{V}) = \text{softmax}\left(\frac{\mathbf{Q}\mathbf{K}^T}{\sqrt{d_k}}\right)\mathbf{V}$$

Encoder Layer Structure

$$\mathbf{z}_l = \text{MSA}(\text{LN}(\mathbf{z}_{l-1})) + \mathbf{z}_{l-1}$$

$$\mathbf{z}_l = \text{FFN}(\text{LN}(\mathbf{z}_l)) + \mathbf{z}_l$$

- Global receptive field from first layer
- $N\times$ encoder layers process image features

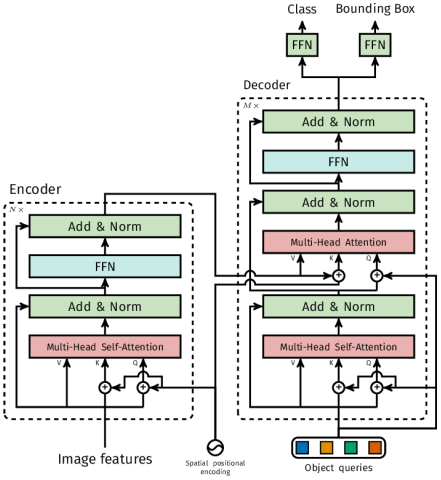

Figure: DETR architecture overview

Step 3: Transformer Decoder & Object Queries

Object Queries

Learnable Detection Slots:

- $N = 100$ learnable embeddings
- $\mathbf{q}_{obj} \in \mathbb{R}^{N \times d}$ (where $d = 256$)
- Each query focuses on different objects
- Learned during training to specialize

Query Initialization:

$$\mathbf{q}_{obj} \sim \mathcal{N}(0, \sigma^2)$$

Decoder Layer

Self-Attention + Cross-Attention:

$$\mathbf{q}_l = \text{SelfAttn}(\text{LN}(\mathbf{q}_{l-1})) + \mathbf{q}_{l-1}$$

$$\mathbf{q}_l = \text{CrossAttn}(\text{LN}(\mathbf{q}_l), \mathbf{z}_{enc}) + \mathbf{q}_l$$

$$\mathbf{q}_l = \text{FFN}(\text{LN}(\mathbf{q}_l)) + \mathbf{q}_l$$

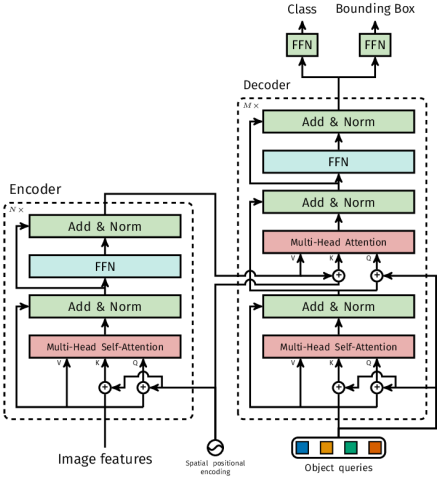

Figure: DETR architecture overview

Step 4: Prediction & Hungarian Matching

Prediction Heads

Classification Head:

$$p_i = \text{softmax}(\text{FFN}_{cls}(\mathbf{q}_i))$$

Box Regression Head:

$$\mathbf{b}_i = \sigma(\text{FFN}_{box}(\mathbf{q}_i))$$

- Each query produces one prediction

Hungarian Algorithm

Bipartite Matching:

$$\hat{\sigma} = \arg\min_{\sigma \in \mathfrak{S}_N} \sum_{i}^{N} \mathcal{L}_{match}(y_i, \hat{y}_{\sigma(i)})$$

Set-based Loss:

$$\mathcal{L} = \sum_{i=1}^{N} [-\log \hat{p}_{\hat{\sigma}(i)}(c_i) + {}_{\{c_i \neq \emptyset\}} \mathcal{L}_{box}(b_i, \hat{b}_{\hat{\sigma}(i)})]$$

The CBIS-DDSM dataset presented several critical inconsistencies requiring systematic correction

Unnecessary Image Regions

- Mammograms contained irrelevant background and metadata areas
- *Solution:* Implemented cropping algorithm (provided by Mr. Yassine Ameskine) to isolate regions of interest
- *Impact:* Focused processing on clinically relevant breast tissue only

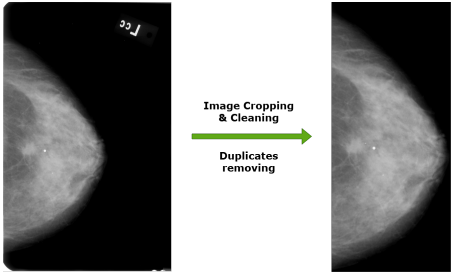

File Corruption and Mismatched Annotations

- Swapped filenames between masks and ROI files
- Missing or deleted mask files
- *Solution:* Developed directory correction algorithm to restore proper file associations and recover masks from ROI

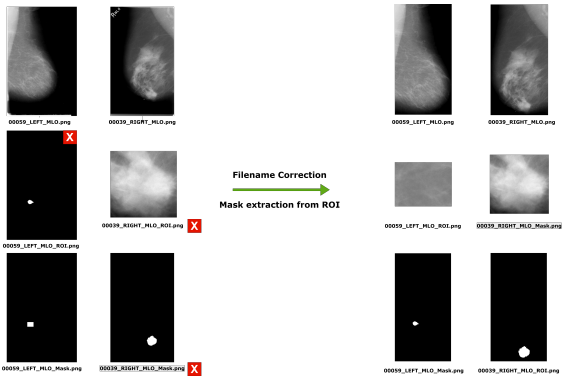

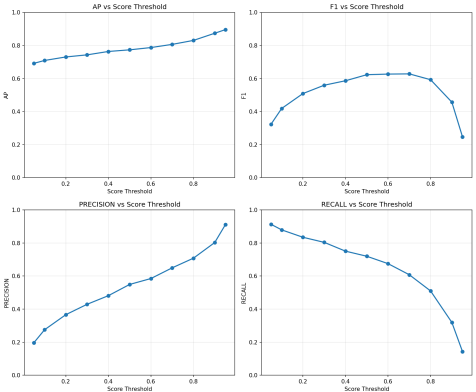

Figure: Performance metrics vs. confidence threshold

- **Optimal Threshold:** 0.7 (F1-maximized)
- **F1-Score:** 0.62
- **Precision:** 0.65
- **Recall:** 0.6
- **High-confidence predictions:** 23.2% above 0.5

Clinical Relevance

Threshold can be adjusted based on screening vs. diagnostic priorities

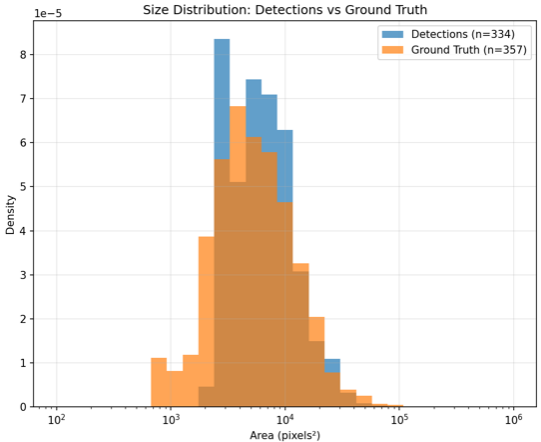

Figure: Predicted vs. ground truth size distributions

- **Detected masses:** 334
- **Ground truth:** 357
- **Size range:** $10^3 - 10^5$ pixels²
- Close distribution alignment

Validation

No bias toward large/small masses
Successful transfer learning